

# Frequency metrology in quantum degenerate helium: Direct measurement of the $2\ ^3S_1 \rightarrow 2\ ^1S_0$ transition

R. van Rooij<sup>1</sup>, J.S. Borbely<sup>1</sup>, J. Simonet<sup>2</sup>, M.D. Hoogerland<sup>3</sup>,  
K.S.E. Eikema<sup>1</sup>, R.A. Rozendaal<sup>1</sup> and W. Vassen<sup>1\*</sup>

<sup>1</sup> LaserLaB Vrije Universiteit, De Boelelaan 1081, 1081 HV Amsterdam, the Netherlands

<sup>2</sup> École Normale Supérieure, Laboratoire Kastler-Brossel, 24 rue Lhomond, 75005 Paris, France

<sup>3</sup> Department of Physics, University of Auckland, Private Bag 92019, Auckland, New Zealand

\* w.vassen@vu.nl

**Precision spectroscopy of simple atomic systems has refined our understanding of the fundamental laws of quantum physics. In particular, helium spectroscopy has played a crucial role in describing two-electron interactions, determining the fine-structure constant and extracting the size of the helium nucleus. Here we present a measurement of the doubly-forbidden 1557-nanometer transition connecting the two metastable states of helium (the lowest energy triplet state  $2\ ^3S_1$  and first excited singlet state  $2\ ^1S_0$ ), for which quantum electrodynamic and nuclear size effects are very strong. This transition is fourteen orders of magnitude weaker than the most predominantly measured transition in helium. Ultracold, sub-microkelvin, fermionic  $^3\text{He}$  and bosonic  $^4\text{He}$  atoms are used to obtain a precision of  $8 \times 10^{-12}$ , providing a stringent test of two-electron quantum electrodynamic theory and of nuclear few-body theory.**

The first observations of helium emission spectra at the end of the 19th century revealed two separate series of lines, associated with orthohelium and parahelium respectively. In 1926 Heisenberg explained the distinction between these two spectra on the basis of wave mechanics, electron spin and the Pauli exclusion principle (1). The spectrum of orthohelium arises from triplet states for which the electron spins are parallel, whereas in parahelium the electron spins are anti-parallel, forming singlet states (Fig. 1). From the lowest state of orthohelium, the  $1s2s\ ^3S_1$  state (denoted  $2\ ^3S_1$ ), only excitations to triplet states have been observed. Orthohelium transitions from the  $2\ ^3S_1$  state and associated studies of the  $n\ ^3P_{0,1,2}$  ( $n=2,3$ ) fine-structure splittings (2–7) have enabled tests of quantum electrodynamics (QED) (8, 9) as well as a determination of the fine-structure constant (5, 10). In the singlet spectrum of helium (parahelium), electric-dipole transitions from the  $1\ ^1S_0$  ground state (11) and from the metastable  $2\ ^1S_0$  state (12, 13) have also provided tests of high-precision QED calculations. All these frequency metrology studies have been performed using either atomic beams or gas discharges. However, helium in the metastable  $2\ ^3S_1$  state (He\*, lifetime  $8 \times 10^3$  s) can be laser cooled and trapped, which allows much longer interaction times for excitation of weak transitions. He\* atoms have been cooled to  $\mu\text{K}$  temperatures, revealing quantum statistical effects of bunching and anti-bunching (14) and achieving quantum degeneracy for both the bosonic isotope  $^4\text{He}$  (15, 16) and the fermionic isotope  $^3\text{He}$  (17).

Here we observe an orthohelium – parahelium transition, specifically, the 1557-nm transition between the metastable  $2\ ^3S_1$  and  $2\ ^1S_0$  states (Fig. 1), both in  $^4\text{He}$  and  $^3\text{He}$ . This transition is an excellent testing ground for fundamental theory of atomic structure. Due to a large electron density at the nucleus, the energy of S-states is the most sensitive to QED and to nuclear size effects (8). For the  $2\ ^3S_1$  and  $2\ ^1S_0$  metastable states, QED terms contribute 4 and 3 GHz respectively, to a total binding energy of  $10^6$  GHz (8, 9). The present accuracy in the QED calculations is 2 MHz, based on an estimate of non-evaluated higher-order terms. Many of these terms are common between the isotopes. Therefore, in the calculation of the isotope shift (i.e., the difference between the transition frequencies for  $^4\text{He}$  and  $^3\text{He}$ ) mass-independent terms cancel and the uncertainty is reduced to the sub-kHz level (18). As the finite nuclear charge radius shifts the  $2\ ^3S_1$  state by 2.6 MHz and the  $2\ ^1S_0$  state by 2.0 MHz, an accurate isotope-shift measurement allows a sensitive determination of the difference in the mean charge radius of the  $\alpha$ -particle and of the  $^3\text{He}$  nucleus, providing a stringent test of nuclear charge radius calculations and experiments (19).

The natural linewidth of the  $2\ ^3S_1 \rightarrow 2\ ^1S_0$  transition is 8 Hz, determined by the 20-ms lifetime of the  $2\ ^1S_0$  state which relaxes via two-photon decay to the ground state (Fig. 1). This transition is 200 000 times narrower than the natural linewidth of the  $2\ ^3P$  state, which is most prominently used for spectroscopy in helium. The Einstein  $A$ -coefficient for the  $2\ ^3S_1 \rightarrow 2\ ^1S_0$  magnetic-dipole transition is  $\sim 10^{-7}\ \text{s}^{-1}$  (20, 21), fourteen orders of magnitude smaller than for the electric-dipole transition from  $2\ ^3S_1$  to  $2\ ^3P_{0,1,2}$  states, which indicates that excitation requires high power and/or long interaction times.

The experiment described here was performed using an apparatus designed for the production of quantum degenerate gases of helium (17, 22). Briefly, the metastable  $2\ ^3S_1$  state is

populated by electron impact in an electric discharge. The atomic beam is collimated, slowed and trapped using standard laser cooling and trapping techniques on the  $2\ ^3S_1 \rightarrow 2\ ^3P_2$  transition at 1083 nm. The atoms, optically pumped to  $m_J=+1$ , are then transferred to a Ioffe-Pritchard type magnetic trap.  $^4\text{He}^*$  atoms are evaporatively cooled towards Bose-Einstein condensation by stimulating radio-frequency (RF) transitions to untrapped states. For  $^3\text{He}^*$  (in the  $F=3/2$  hyperfine state), quantum degeneracy is reached by sympathetic cooling with  $^4\text{He}^*$ . Either one, or both, of the two isotopes are transferred into a crossed-beam optical dipole trap. This trap consists of two focused 1557-nm laser beams, intersecting at their foci as shown in Fig. 2. We transfer up to  $10^6$  atoms to this optical trap.

After loading the optical trap, the atoms are illuminated by a separate beam for spectroscopy which is derived from the same laser as the optical trap beam, but is switched and frequency shifted by a 40-MHz acousto-optic modulator. A heterodyne signal is set up between the 1557-nm laser and a mode of a femtosecond frequency comb laser to deduce the absolute frequency of the spectroscopy laser. The frequency comb is based on a mode-locked erbium-doped fiber laser, for which both the repetition rate and the carrier-envelope-offset frequency are referenced to a GPS-controlled Rubidium clock (23).

After a certain interaction time (typically 1 to 6 s), both the spectroscopy beam and the trap beam are switched off, allowing the atoms to fall due to gravity. The high internal energy of  $\text{He}^*$  (20 eV above the  $1\ ^1S_0$  ground state) allows for efficient detection on a microchannel plate (MCP) detector (Fig. 2). The MCP signal reflects both the number of atoms and their temperature. In the case of  $^4\text{He}$ , the signal has a bimodal character that results from the combination of Bose-condensed atoms and thermal atoms (Fig. 3(a)); a fit to this signal provides the number of condensed atoms (23). Because the excited state is anti-trapped, the trap is depleted when the spectroscopy beam is resonant with the atomic transition. By deducing the remaining number of  $2\ ^3S_1$  atoms for various laser frequencies, the atomic resonance frequency is determined from a Gaussian fit to the data (Fig. 3(b)). The observed linewidth is largely due to the 75-kHz laser linewidth.

Several systematic shifts in the transition frequency are taken into account (23). The largest shift is due to the Zeeman effect. The measured transition,  $2\ ^3S_1 (m_J=+1) \rightarrow 2\ ^1S_0 (m_J=0)$  for  $^4\text{He}$ , and  $2\ ^3S_1, F=3/2 (m_F=+3/2) \rightarrow 2\ ^1S_0, F=1/2 (m_F=+1/2)$  for  $^3\text{He}$ , is shifted from resonance predominantly by the Earth's magnetic field. The size of the shift is deduced by measuring the resonance frequency of RF spin-flip transitions between the  $2\ ^3S_1$  magnetic sub-states. An additional shift is caused by the momentum transfer from a 1557-nm photon to an atom. In the case of  $^4\text{He}$ , the high density of the condensate could potentially cause a mean-field shift (24). However, by performing the experiment with reduced atomic density, no shift is observed.

The second largest systematic frequency perturbation is due to the AC Stark shift associated with the intense 1557-nm light which induces the dipole trap: the specific energy state of the trapping potential for an atom determines the AC Stark shift for that atom. For  $^4\text{He}$ , only excitations of atoms condensed in the ground state of the dipole trap are taken into account in determining the transition frequency. As the trap depth depends linearly on laser intensity,

measuring the resonance frequency for a range of applied laser powers allows an extrapolation to zero laser intensity. In contrast,  $^3\text{He}$  atoms, due to their fermionic nature, are distributed throughout the energy states of the dipole trap and as a result the measured AC Stark shift does not equal the trap depth (as is the case with  $^4\text{He}$ ), but is reduced due to the density of states within the dipole trap. A non-linear shift can then potentially arise at high laser intensities, where the larger trap depths allow for higher temperatures. To minimize this effect  $^3\text{He}$  atoms are sympathetically cooled to the quantum degenerate regime to predominantly populate the lowest energy states of the trapping potential. Over the course of several months, 20 independent extrapolations were obtained (as shown in Fig. 4) to deduce an absolute frequency of the  $2\ ^3\text{S}_1 \rightarrow 2\ ^1\text{S}_0$  transition for  $^4\text{He}$  of  $f_4 = 192\ 510\ 702\ 145.6(1.8)$  kHz and for  $^3\text{He}$  ( $F=3/2 \rightarrow F=1/2$ ) of  $f_3 = 192\ 504\ 914\ 426.4(1.5)$  kHz, where the one standard deviation error in parentheses includes all statistical and systematic uncertainties.

For both isotopes, our result agrees with QED calculations of the ionization energies of the two metastable states (9, 25). The present experimental error in the transition frequency is three orders of magnitude smaller than estimates of non-evaluated higher-order terms in state-of-the-art QED calculations and presents a significant challenge for groups involved in atomic structure theory.

An indirect value of the energy difference between the  $2\ ^3\text{S}_1$  and the  $2\ ^1\text{S}_0$  states can be obtained from the literature (only for  $^4\text{He}$ ) by combining experimental transition frequencies from both metastable states to high-lying S, P and D states with theoretical values for the ionization energies of these states. This procedure yields ionization energies for the  $2\ ^1\text{S}_0$  state (8, 12, 13) and the  $2\ ^3\text{S}_1$  state (2, 8) and the difference between these values gives a transition frequency of  $192\ 510\ 701.96(16)$  MHz, in agreement with our result though with hundred-fold lower precision.

Isotope shift measurements, combined with high-precision QED theory, provide a method to isolate contributions due to finite nuclear size effects. The difference in nuclear charge radii between  $^3\text{He}$  and  $^4\text{He}$  is determined by comparing experiment and theory. Because the  $^4\text{He}$  nuclear charge radius is the most precisely known radius of all nuclei determined from electron scattering experiments (26),  $1.681(4)$  fm, a value of the  $^3\text{He}$  nuclear charge radius with similar precision can be deduced. In calculating the isotope shift, QED theory is more precise than our measurement as mass-independent terms cancel. The theoretical value for the isotope shift (assuming point-like nuclei) is  $8\ 034\ 148.6(7)$  kHz (23). Subtracting the measured transition frequencies and correcting for the accurately-known hyperfine structure (25, 27), we find an isotope shift of  $f_4 - f_3 + f_{hfs} = 8\ 034\ 367.2(2.3)$  kHz. The 218.6 kHz difference may be attributed to the finite size of both nuclei. This nuclear shift is proportional to the difference in the nuclear charge radii squared,  $\Delta r_c^2 \equiv r_c^2(^3\text{He}) - r_c^2(^4\text{He})$ . Using the theoretical proportionality constant of  $4.6642\ \text{fm}^2/\text{MHz}$  (18) for the measured transition, we deduce  $\Delta r_c^2 = 1.019(11)\ \text{fm}^2$ .  $\Delta r_c^2$  represents a more universal parameter than the value of the isotope shift as it is obtained from various branches of physics. Besides through spectroscopic means, it can be determined from nuclear theory and from electron-scattering experiments. Nuclear few-body theory provides  $\Delta r_c^2 = 1.16 \pm 0.12\ \text{fm}^2$  (18, 23, 28), whereas from electron-scattering

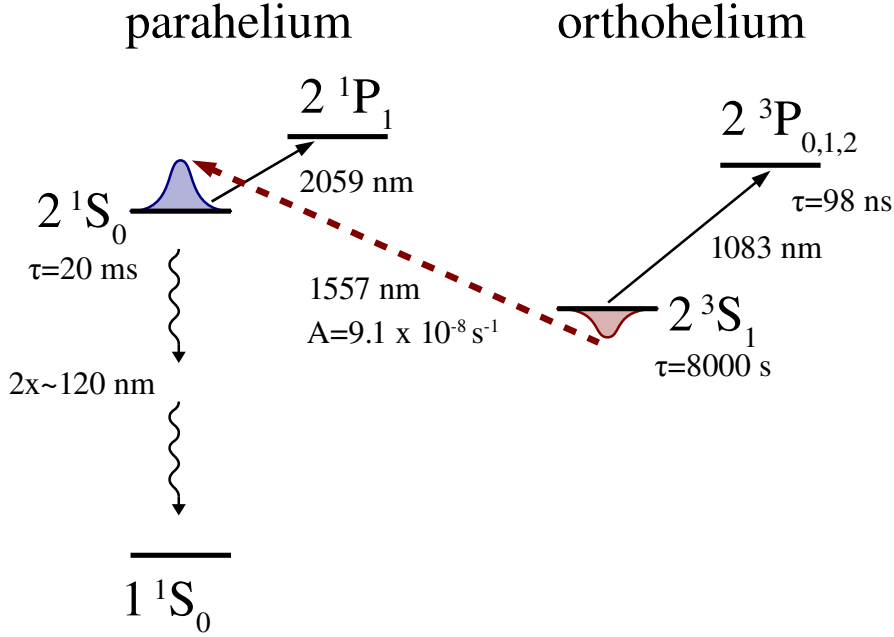


Figure 1: Relevant energy levels, transition wavelengths and state lifetimes of helium. The magnetic-dipole transition connecting the  $2^3S_1$  state and the  $2^1S_0$  state has a wavelength of 1557 nm and an Einstein-A coefficient of  $9.1 \times 10^{-8} \text{ s}^{-1}$ . A focused 1557-nm laser also constitutes a trap for ultracold atoms in the  $2^3S_1$  state because it is red detuned from the  $2^3S_1 \rightarrow 2^3P_J$  transitions. As the 1557-nm laser light is blue detuned from the  $2^1S_0 \rightarrow 2^1P_1$  transition, atoms in the  $2^1S_0$  state are anti-trapped.

experiments  $\Delta r_c^2 = 1.01 \pm 0.13 \text{ fm}^2$  (26, 29). Comparing the values of  $\Delta r_c^2$ , we find our result to be in good agreement but an order of magnitude more precise. An independent spectroscopic measurement in helium on the  $2^3S_1 \rightarrow 2^3P_0$  transition (30) gives  $\Delta r_c^2 = 1.059(3) \text{ fm}^2$ , obtained using the most recent QED calculations (19). Although the measurement precision of the isotope shift for this transition is comparable to our precision, the smaller uncertainty in  $\Delta r_c^2$  is due to a larger sensitivity to differential nuclear charge effects. Presently, the accuracy to which the  $^4\text{He}$  charge radius is known sets a lower limit on the uncertainty of the  $^3\text{He}$  charge radius determined from helium spectroscopy. Our measurement presents a value for the  $^3\text{He}$  nuclear charge radius of 1.961(4) fm.

We have also demonstrated that all of the trapped atoms can be transferred to the  $2^1S_0$  state, producing a source of ultracold singlet helium. Optically trapping these atoms simultaneously with cold  $1^1S_0$  ground state atoms (produced after two-photon decay) opens up the possibility to perform two-photon spectroscopy on the  $2^1S_0 \leftrightarrow 1^1S_0$  transition (11, 31), where QED and nuclear size effects are strongest.

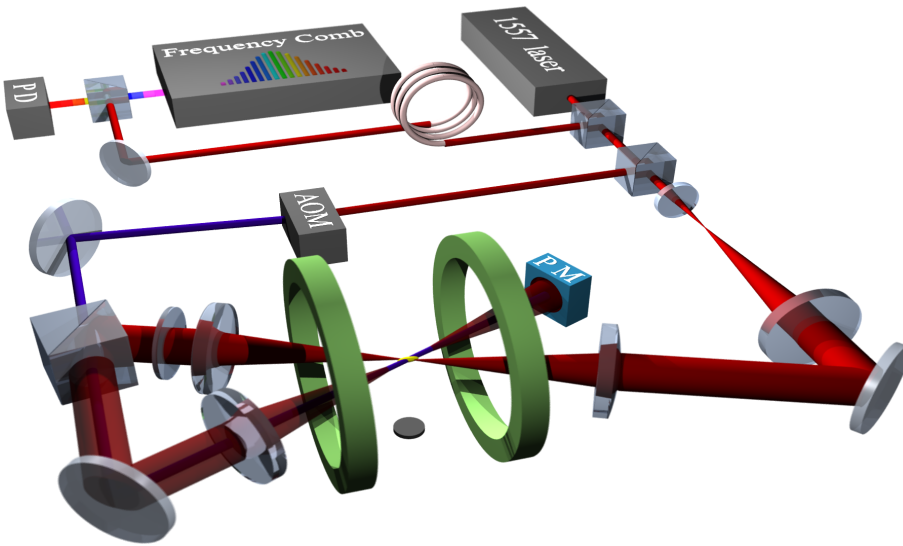


Figure 2: Experimental setup. A small fraction of the 1557-nm laser light is split off and coupled via a fiber-optic link to be referenced to a fiber-based frequency comb. A heterodyne signal is monitored on a fast photodiode (PD) to determine the absolute frequency of the 1557-nm laser. The remaining light is divided into the trap beam and the spectroscopy beam. A crossed-beam dipole trap configuration is realized by focusing both the incident and returning trap beam (with orthogonal linear polarizations) to a waist of  $\sim 85 \mu\text{m}$  at the center of the magnetic trap (represented by the green coils) under a relative angle of 19 degrees, trapping atoms at the intersection. The spectroscopy beam is frequency shifted by a 40-MHz acousto-optical modulator (AOM), overlapped with the returning trap beam and absorbed by a thermopile power meter (PM). A microchannel plate detector is positioned underneath the trap for temperature and atom number determination.

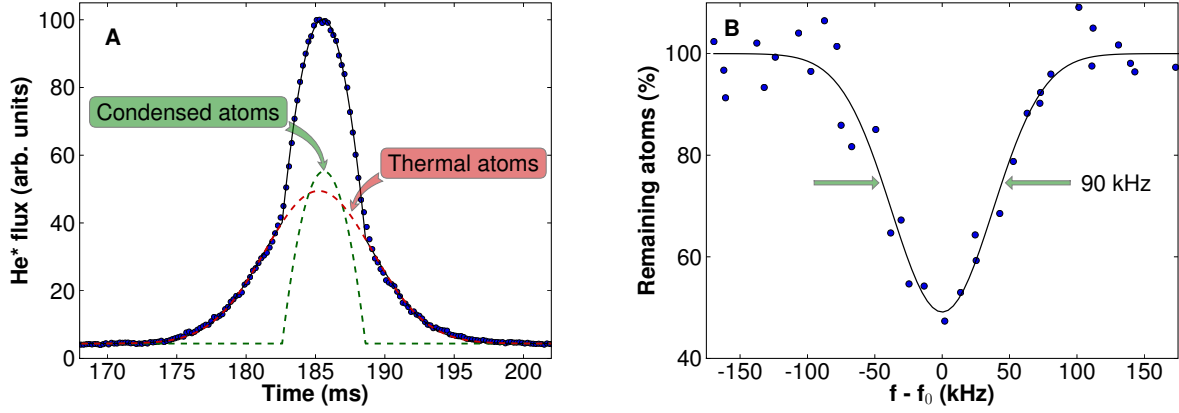


Figure 3: **(A)** Bimodal time-of-flight distribution observed when He\* atoms are detected on the MCP detector approximately 186 ms after the trapping laser light is turned off. The MCP signal is fit to determine the number of Bose-condensed atoms. **(B)** The percentage of Bose-condensed  $^4\text{He}$  atoms remaining in the  $2\ ^3\text{S}_1$  state as a function of applied laser frequency (relative to the fitted center frequency  $f_0$ ). The line is a fit of a Gaussian to the data. We measure linewidths varying from 75 to 130 kHz depending on the trap depth and on the isotope.

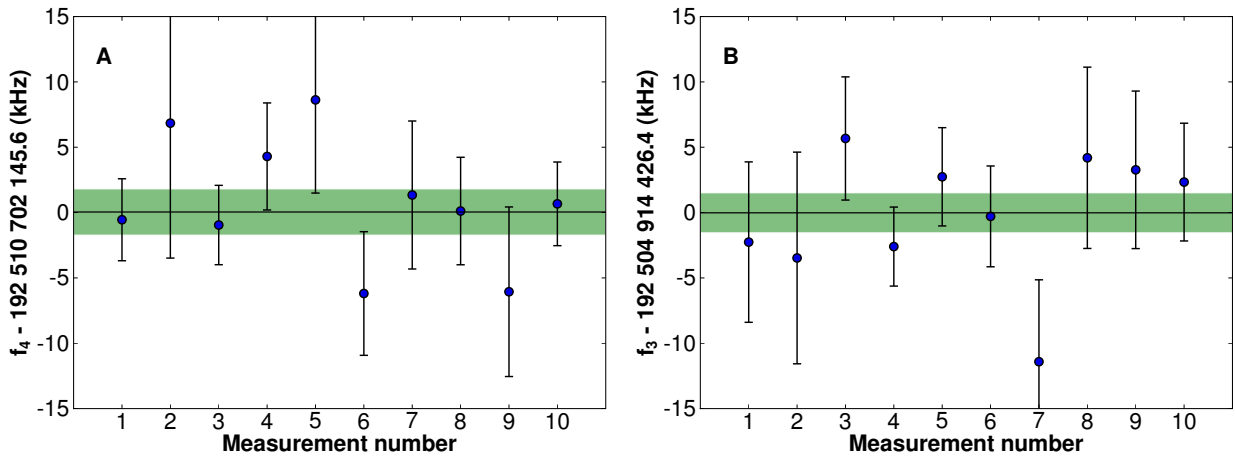


Figure 4: Measured transition frequencies for  $^4\text{He}$  **(A)** and for  $^3\text{He}$  **(B)**. The error bar on each data point includes contributions from various systematics, e.g. AC Stark shift and Zeeman shift (23). The frequencies quoted on the y-axes are the weighted averages of the data points. Their associated uncertainties (with the uncertainties due to the frequency comb calibration and the mean field shift added in quadrature) are  $\pm 1.8$  kHz for  $^4\text{He}$  and  $\pm 1.5$  kHz for  $^3\text{He}$ , represented by the green bands.

# SUPPORTING ONLINE MATERIAL

## Experimental details

The 1557-nm laser beam is generated by an NP-Photonics erbium-doped CW fiber laser (Scorpio), which has a specified short-term spectral linewidth of  $< 5$  kHz and has a piezoelectric input for fast frequency tuning. The power used for the optical trap is variable and is measured on a thermopile power meter. The minimum power required to trap atoms is 15 mW and the maximum used is 250 mW, which corresponds to a trap depth ranging from 0.3 to 5  $\mu$ K, and axial and radial trap frequencies ranging from  $(\omega_{ax}, \omega_{rad}) = 2\pi \times (20, 140)$  Hz to  $2\pi \times (80, 570)$  Hz. The lifetime of atoms in the trap is limited by background collisions to approximately 15 s. After being loaded into the optical trap, the atoms are illuminated by the spectroscopy beam. This beam has a waist of 280  $\mu$ m at the position of the atoms, much larger than the cloud size. A measure for the number of atoms is obtained by letting the atoms fall onto a microchannel plate (MCP) detector, located 17 cm below the trap center. The MCP signal (Fig. 3(a)) shows an integrated time-of-flight trace of the atoms as they hit the detector. In the case of  $^4\text{He}$  the signal shows a bimodal character, which is fitted with a linear combination of a gaussian and a parabolic function, representing the thermal atoms and Bose-condensed atoms respectively (15, 22). For  $^3\text{He}$ , a Fermi-Dirac time-of-flight function is used to fit the MCP signal (17).

## Systematic shifts and uncertainties

To obtain the value of the transition frequency several systematic shifts need to be evaluated, i.e., the AC Stark shift, the Zeeman shift, the recoil shift and, in case of a Bose-Einstein condensate a mean-field shift. A summary of the systematic uncertainties are shown in Table S1. The systematic shifts and uncertainties are discussed in detail below.

Table S1: Combined systematic and statistical uncertainties. Units are kHz.

	$^4\text{He}$	$^3\text{He}$
Frequency comb	0.4	0.4
Zeeman shift	0.5	0.5
Mean-field shift	1.1	
Recoil shift	0.0	0.0
AC Stark shift extrapolation	1.4	1.4
Total (in quadrature)	1.8	1.5

*Frequency comb.* The 1557-nm laser frequency is locked to a frequency comb based on a mode-locked erbium-doped fiber laser (Menlo Systems), for which both the repetition rate and the carrier-envelope-offset frequency are referenced to a GPS-controlled Rubidium clock (PRS10

Stanford Research). The frequency comb has a long-term frequency stability of better than one part in  $10^{12}$ . The beat frequency between the 1557-nm laser and one of the comb modes is measured on a fast photo-diode. The  $n^{\text{th}}$  comb mode producing the lowest frequency beat with the 1557-nm laser is the one for which  $n$ -times the repetition rate ( $f_{rep} \approx 250$  MHz) of the comb laser plus the carrier-envelope-offset frequency ( $f_{ceo} = 20$  MHz) matches the 1557-nm laser frequency most closely, then  $f_{1557\text{ nm}} = f_{ceo} + n f_{rep} \pm f_{beat}$ . In order to determine the absolute frequency of the spectroscopy laser the specific comb-mode number  $n$  is determined using an accurately calibrated wave meter. The beat frequency of the 1557-nm laser with the frequency comb is continuously measured and regulated by a feed-back loop to match a set-point frequency. The integration time is 30 ms, which is a trade-off between the averaging time of the comb laser and the short-term stability of the spectroscopy laser. This laser locking scheme results in a long-term laser linewidth of 75 kHz (FWHM). For each instance of measuring the  $2^3\text{S}_1 \rightarrow 2^1\text{S}_0$  transition frequency 40 different values of  $f_{beat}$  are chosen, where the interaction time between the spectroscopy laser and the atoms is, on average, 3 seconds. This corresponds to a total interaction time of 120 seconds which results in an expected uncertainty of the calibration with the frequency comb of less than 0.4 kHz.

*Zeeman shift.* The transition frequency is shifted by the differential Zeeman shift of the initial and the final state in a residual magnetic field, the magnitude of which is approximately 0.5 G, predominantly due to Earth's magnetic field. In a field this size, only first-order Zeeman effects are of relevance at the precision of our experiment.  $^4\text{He}$  atoms are initially in the  $2^3\text{S}_1$  ( $m_J=+1$ ) state, introducing a shift rate of  $g_s\mu_B/h = 2.8025$  MHz/G, where  $h$  is the Planck constant,  $g_s$  is the electron g-factor and  $\mu_B$  is the Bohr magneton. The final state is  $2^1\text{S}_0$  ( $m_J=0$ ), which does not shift due to the absence of a magnetic moment. In the case of  $^3\text{He}$ , both the initial and final states have an additional nuclear spin contribution. The initial  $2^3\text{S}_1$ ,  $F=3/2$  ( $m_F=+3/2$ ) state shifts by  $(g_s\mu_B - \frac{1}{2}g_i\mu_N)/h$ , where  $g_i$  is the nuclear g-factor and  $\mu_N$  is the nuclear magneton. The final state,  $2^1\text{S}_0$ ,  $F=1/2$  ( $m_F=+1/2$ ), shifts by  $-\frac{1}{2}g_i\mu_N/h$ . As such, the differential shift rate is  $g_s\mu_B/h$ , equal to that of  $^4\text{He}$ .

For both  $^4\text{He}$  and  $^3\text{He}$ , the Zeeman shift is determined by inducing radio-frequency (RF) transitions to the  $m_J=0$  and  $m_J=-1$  magnetic substates in  $^4\text{He}$  (Fig. S1). After a 40- $\mu\text{s}$  RF pulse at a set frequency, the atoms are released from the dipole trap and the spin-state populations are separated during time-of-flight in an applied magnetic field gradient. Subsequently, an absorption image is taken from which the relative populations of the magnetic substates are obtained. The Zeeman shift equals the frequency for which most atoms are transferred. On average, the uncertainty of the value we deduce for the Zeeman shift using this procedure is 0.5 kHz.

Zeeman shift measurements are performed intermittently with  $2^3\text{S}_1 \rightarrow 2^1\text{S}_0$  transition measurements in order to compensate for slow changes in the magnetic field. The standard deviation of the value of the Zeeman shift over the course of a day is, on average, 2 kHz which corresponds to a stability of the magnetic field of  $\pm 0.7$  mG.

*Mean-field shift.* An additional correction to the transition frequency for  $^4\text{He}$  is the cold col-

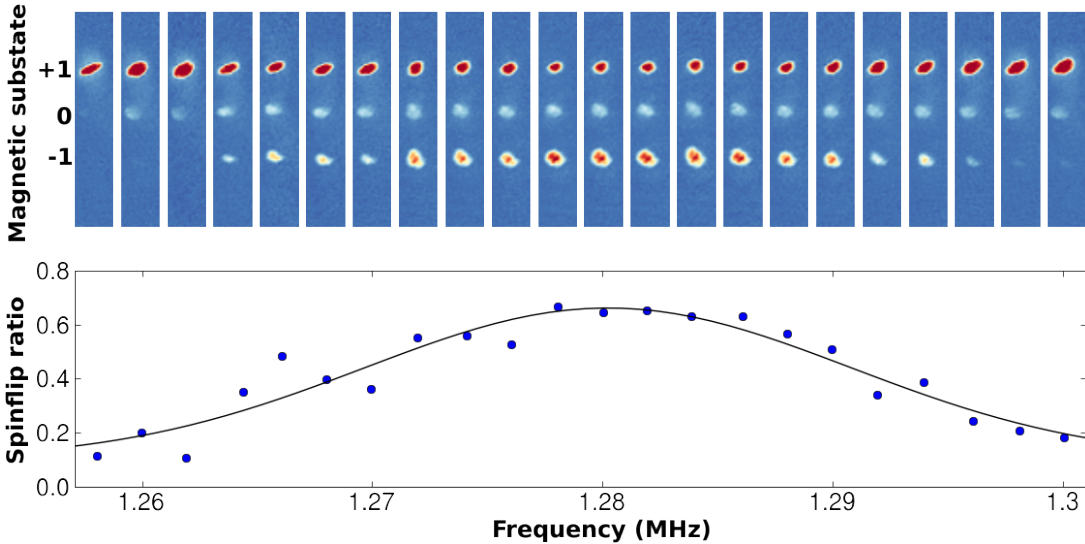


Figure S1: Measurement of the Zeeman shift. The images show the population of magnetic substates of the  $2^3S_1$  manifold after a Stern-Gerlach type experiment as a function of applied microwave frequency. The ratio of atoms in the  $m_J=0$  and  $m_J=-1$  state versus atoms in the  $m_J=1$  state is plotted in the graph. A fit provides the resonance frequency which equals the Zeeman shift.

lision frequency shift (24). Originating from the difference in mean-field energy between the ground state and the excited state, this frequency shift is proportional to the density of trapped atoms and to the difference in  $s$ -wave scattering lengths for the triplet-triplet and the triplet-singlet molecular potentials. The triplet-triplet scattering length is  $+7.5$  nm (32); however, the value of the triplet-singlet scattering length is presently unknown. By measuring the  $2^3S_1 \rightarrow 2^1S_0$  transition frequency with a high atomic density and with a low atomic density (reduced by a factor of 5) and taking the difference, we find a mean-field shift of  $0.07 \pm 1.08$  kHz which is consistent with no mean-field shift to within 1.1 kHz.

*Recoil shift.* Due to momentum conservation, when an atom is excited from the  $2^3S_1$  state to the  $2^1S_0$  state, the momentum of the atom is increased by the momentum of the absorbed photon:  $\Delta p = hf/c$ , where  $h$  is the Planck constant,  $f$  is the photon frequency and  $c$  is the speed of light. The corresponding increase in kinetic energy for the atom must come from the photon, leading to a recoil shift of  $\Delta E = \frac{1}{2m} \left(\frac{hf}{c}\right)^2$ , where  $m$  is the atomic mass. For a  $^4\text{He}$  atom excited by a 1557-nm photon, the recoil shift is 20.6 kHz and for  $^3\text{He}$  it is 27.3 kHz, with negligible uncertainty.

*AC Stark shift extrapolation.* The AC Stark shift is linearly proportional to the sum of the power in the trap and spectroscopy beams. The trap-to-spectroscopy power ratio is fixed, but the total power is variable and measured on a thermopile power meter. The atomic transition is measured

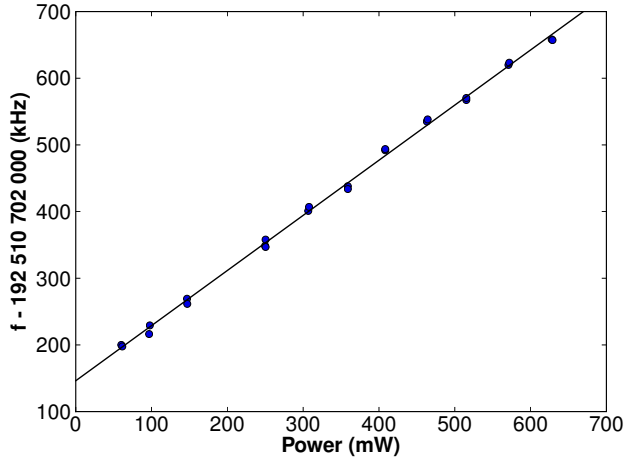


Figure S2: Measured transition frequency for  $^4\text{He}$  as a function of total laser power. The resonance frequency is AC-Stark shifted as power increases. The field-free transition frequency is found at the point where the fitted line crosses the vertical axis. Each data point is obtained by performing several measurements and corrected for the Zeeman shift and for the recoil shift.

several times at a single power and then repeated for a range of powers, as shown in Fig. S2 for  $^4\text{He}$ . From a linear fit, the extrapolation to a field-free resonance frequency is deduced. On average, one extrapolation gives an uncertainty of 5 kHz. In total, 10 extrapolations are determined for  $^4\text{He}$  and for  $^3\text{He}$ , reducing the final uncertainties to 1.3 kHz.

The thermopile power meter readings are corrected for non-linearity by applying a bench-top calibration procedure. The uncertainty in this calibration procedure contributes an additional uncertainty of 0.6 kHz, leading to a combined uncertainty in the AC Stark shift extrapolation of 1.4 kHz.

### Theoretical determination of ionization energies

*Indirect determination.* Combining experimental transition frequencies from both metastable states to higher S, P and D states with theoretical values for the ionization energies of these states yields ionization energies 960 332 041.01(15) MHz for the  $2^1\text{S}_0$  state (8, 12, 13) and 1 152 842 742.97(6) MHz for the  $2^3\text{S}_1$  state (2, 8). Combining these values a  $2^3\text{S}_1 \rightarrow 2^1\text{S}_0$  transition frequency of 192 510 701.96(16) MHz is deduced for  $^4\text{He}$ .

*QED theory.* QED calculations of ionization energies of the two metastable states of  $^4\text{He}$  presently agree between different theory groups (8, 9), although their calculations are not fully independent. Drake and Yan (8) find 960 332 037.9(1.7) MHz and 1 152 842 741.3(2.5) MHz for the ionization energies of  $2^1\text{S}_0$  and  $2^3\text{S}_1$  respectively, whereas Yerokhin and Pachucki (9) find 960 332 038.0(1.9) MHz and 1 152 842 741.4(2.6) MHz. This implies a theoretical tran-

sition frequency of 192 510 703.4(2.6) MHz (for both theory groups), where we took the maximum of the theoretical uncertainties of both ionization energies as the uncertainty in the transition frequency since both uncertainties are expected to be correlated (private communication, K. Pachucki and V. Yerokhin, 2010). The uncertainty is due to approximations made in calculating all higher-order  $\alpha^7$  terms in QED, where  $\alpha$  is the fine-structure constant.

*Isotope shift.* From Table 2 of Ref. (18), the differences in ionization energies between  ${}^3\text{He}$  and  ${}^4\text{He}$  are 45 862 986.0(5) kHz for the  $2\ {}^1\text{S}_0$  state and 53 897 130.1(6) kHz for the  $2\ {}^3\text{S}_1$  state. Recently, Drake corrected a sign error in this calculation leading to corrected values of 45 862 980.9(7) kHz and 53 897 129.4(8) kHz respectively (private communication Drake 2010). These values agree with the isotope shifts of the ionization energies as calculated by Pachucki and Yerokhin (private communication, 2010): 45 862 979.58 kHz and 53 897 128.33 kHz respectively. The latter values were calculated applying the methodology of Ref. (9). All these values exclude hyperfine structure effects and contributions due to finite nuclear size effects, i.e. assuming point charge radii. Taking the difference between the isotope shifts of the  $2\ {}^1\text{S}_0$  and  $2\ {}^3\text{S}_1$  ionization energies, the calculated isotope shift for the atomic transition by Drake is 8 034 148.5(7) kHz and by Yerokhin and Pachucki is 8 034 148.75(69) kHz, where the uncertainty is estimated to be about 20% of the E61 term which is a sum of pure recoil and radiative recoil corrections of  $\mathcal{O}(\alpha^6 m^2/M)$ , where  $m$  is the electron mass and  $M$  is the nuclear mass. For our calculation of the nuclear shift we use the average of the theoretical isotope shifts: 8 034 148.63(70) kHz. The hyperfine structure of  ${}^3\text{He}$  (25) shifts the  $2\ {}^3\text{S}_1\ F=3/2$  state by -2 246 587.3 kHz and the  $2\ {}^1\text{S}_0\ F=1/2$  state by 60.6 kHz (due to hyperfine-induced singlet-triplet mixing).

### Helium charge radii from nuclear theory

Equation 29 from Ref. (18) relates the nuclear charge radius to an effective rms radius of the nucleus (corresponding to the distribution of point-like protons and neutrons in the nucleus), to the mean-charge radius of the proton and to the mean-charge radius of the neutron. The effective rms radius is taken from Tables 7 and 8 of Ref. (28). The results given in these Tables correspond to state-of-the-art calculations of nucleon-nucleon and three-nucleon forces.

## References and Notes

1. W. Heisenberg, *Z. Phys.* **39**, 499 (1926).
2. C. Dorrer, F. Nez, B. de Beauvoir, L. Julien, F. Biraben, *Phys. Rev. Lett.* **78**, 3658 (1997).
3. P. C. Pastor, *et al.*, *Phys. Rev. Lett.* **92**, 023001 (2004).
4. P. Mueller, *et al.*, *Phys. Rev. Lett.* **94**, 133001 (2005).
5. M. Smiciklas, D. Shiner, *Phys. Rev. Lett.* **105**, 123001 (2010).
6. J. S. Borbely, *et al.*, *Phys. Rev. A* **79**, 060503 (2009).
7. T. Zelevinsky, D. Farkas, G. Gabrielse, *Phys. Rev. Lett.* **95**, 203001 (2005).
8. G. W. F. Drake, Z.-C. Yan, *Can. J. Phys.* **86**, 45 (2008).
9. V. A. Yerokhin, K. Pachucki, *Phys. Rev. A* **81**, 022507 (2010).
10. K. Pachucki, V. A. Yerokhin, *Phys. Rev. Lett.* **104**, 070403 (2010).
11. D. Kandula, *et al.*, *Phys. Rev. Lett.* **105**, 063001 (2010).
12. C. J. Sansonetti, J. D. Gillaspy, *Phys. Rev. A* **45**, R1 (1992).
13. W. Lichten, D. Shiner, Z.-X. Zhou, *Phys. Rev. A* **43**, 1663 (1991).
14. T. Jelte, *et al.*, *Nature* **445**, 402 (2007).
15. A. Robert, *et al.*, *Science* **292**, 461 (2001).
16. F. Pereira Dos Santos, *et al.*, *Phys. Rev. Lett.* **86**, 3459 (2001).
17. J. M. McNamara, T. Jelte, A. S. Tychkov, W. Hogervorst, W. Vassen, *Phys. Rev. Lett.* **97**, 080404 (2006).
18. G. W. F. Drake, W. N. Nörtershäuser, Z.-C. Yan, *Can. J. Phys.* **83**, 311 (2005).
19. D. C. Morton, Q. Wu, G. W. F. Drake, *Phys. Rev. A* **73**, 034502 (2006).
20. G. Łach, K. Pachucki, *Phys. Rev. A* **64**, 042510 (2001).
21. K. A. H. van Leeuwen, W. Vassen, *Europhys. Lett.* **76**, 409 (2006).
22. A. S. Tychkov, *et al.*, *Phys. Rev. A* **73**, 031603 (2006).
23. Methods and calculations are further detailed in supporting material at *Science Online*.

24. T. C. Killian, *et al.*, *Phys. Rev. Lett.* **81**, 3807 (1998).
25. D. C. Morton, Q. Wu, G. W. F. Drake, *Can. J. Phys.* **84**, 83 (2006).
26. I. Sick, *Phys. Rev. C* **77**, 041302 (2008).
27. S. D. Rosner, F. M. Pipkin, *Phys. Rev. A* **1**, 571 (1970).
28. A. Kievsky, S. Rosati, M. Viviani, L. E. Marcucci, L. Girlanda, *J. Phys. G* **35**, 063101 (2008).
29. I. Sick, *Lect. Notes Phys.* **745**, 57 (2008).
30. D. Shiner, R. Dixson, V. Vedantham, *Phys. Rev. Lett.* **74**, 3553 (1995).
31. E. Eyler, *et al.*, *Eur. Phys. J. D* **48**, 43 (2008).
32. S. Moal, *et al.*, *Phys. Rev. Lett.* **96**, 023203 (2006).
33. This work, as part of the European Science Foundation EuroQUAM Programme, was financially supported by the Dutch Foundation for Fundamental Research on Matter (FOM). J.S. acknowledges financial support from the EC's Seventh Framework Programme (LASERLAB-EUROPE). M.D.H. and K.S.E.E acknowledge financial support from the Netherlands Organisation for Scientific Research (NWO). We would like to thank J. Bouma for technical support, and J. Koelemeij and T. van Leeuwen for fruitful discussions. We also thank G. Drake, K. Pachucki, and V. Yerokhin for sharing the calculated theoretical parameters detailed in SOM.